Digest Journal of Nanomaterials and Biostructures Vol. 16, No. 1, January - March 2021, p. 271 - 282

SYNTHESIS AND CHARACTERIZATION OF Ce DOPED ZnO TWO-DIMENSIONAL NANOSHEETS FOR VISIBLE LIGHT PHOTOCATALYTIC DEGRADATION OF MB

Q. SHEN, M. H. XU*, G. XIANG PAN, S. L. LAI, Y. H. TONG
Department of Materials Engineering, Huzhou University, Huzhou 313000, P. R. China

Ce doped ZnO fish-scale shaped two-dimensional nanosheets photocatalysts (Ce-ZnO) were successfully prepared via hydrothermal method. The Ce-ZnO nanostructures were characterized by SEM, EDS, XRD, and UV-Vis DRS techniques. Ce ions were successfully incorporated into the lattice position of ZnO with Ce molar ratio lower than 1%. The photocatalytic capacity of Ce-doped ZnO nanosheets for removal of methylene blue (MB) were evaluated by batch experiment under visible light irradiation. The results revealed that the 1% mole ratio of Ce doped ZnO sample exhibited the highest photocatalytic efficiency for methylene blue (MB), where 96.48% of MB was degraded at 60 min.

(Received November 15, 2020; Accepted March 8, 2021)

Keywords: Photocatalysis, Ce, Doped, ZnO, Two-dimensional nanosheets, Methylene blue

1. Introduction

Organic contaminants in waste water not only pollute the ecological environment, but also endanger the public health of mankind. People have spent great efforts on removing the organic compounds from the waste water. Semiconductor photocatalytic degradation of water treatment has been recognized as a promising technology because it is effective, low-cost, environment-friendly and able to utilize the solar energy directly [1, 2]. ZnO is a superior semiconductor material for photocatalysis. ZnO has unique advantages, such as, high electron mobility and adjustable morphology. However, the bandgap of ZnO is relatively big (3.37eV) and only ultraviolet light can be absorbed, which accounts for only 4% of the solar spectrum [3]. In addition, fast recombination of photogenerated election/hole and low photocatalytic stability are common drawbacks of ZnO [4-6]. Therefore, researchers have made a lot of efforts to improve the photocatalysis capability of ZnO by various methods.

Doping is an important approach for ZnO modification. The introduction of mental atoms into the lattice of ZnO can adjust the band gap and improve the utilization of solar light as well as tailor ZnO nanostructures [7-15]. Mental elements, such as Cu [7, 8], Fe [9], La [10], Al [11], Gd [12], Sb [13] and Ag [14] have been reported for doping of ZnO. As one of rare earth metals, Cerium(Ce) has attracted much attention due to its outstanding advantages: 4f electron transition and abundant energy levels [16, 17]. Doping of Ce in ZnO achieves great improvement of the photocatalytic activity. Flower-like mesoporous Ce-ZnO nanosheets [16] was prepared by a one-step wet chemical method. 1% Ce doped ZnO exhibited highest photocatalytic activities with 85.1% removal of RhB under irradiation of stimulated sunlight and the photocatalytic performance increased to 89.5% after annealing at 500°C. Chang et al. [18] synthesized Ce dopd ZnO nanorods with excellent visible-light catalytic activity by using hydrothermal method. Doping of Ce increased surface oxygen vacancies and leaded to red-shift for visible light absorption of ZnO. Sukriti [19] fabricated $Zn_{1-x}Ce_xO$ nanostructures via co-precipitation method. The nanostructures changes from

* Corresponding author: xumh123@163.com

nanocubes to nanobars and nanohexanes with the increase of doped Ce^{3+} concentration. The band gap of Ce doped ZnO shifted from 3.17eV to 2.72eV and The Zn0.94Ce0.6O showed 94.11% degradation of Methylene blue (MB). Jiang [20] reported that the photocatalytic methyl orange (MO) degradation efficiency of Ce-doped ZnO hollow sphere reached 99% under irradiation of 500W Xenon lamp. However, the preparation methods mentioned above are either multi-step or high-energy-costing. Meanwhile, it is of great importance to explore simpler and cheaper synthesis methods of Ce-ZnO nanostructures with higher photocatalytic performance. The purpose of this work is to develop a facile approach for Ce-doped ZnO preparation. Methylene blue (MB) is selected as organic containments. The degradation process and mechanism were investigated as well.

2. Experimental

2.1. Materials and chemicals

$Zn(Ac)_2{\cdot}2H_2O$, $Ce(NO_3)_2{\cdot}6H_2O$, urea and cetyltrimethylammonium bromide (CTAB) were obtained from Shanghai Aladdin Biochemical Technology Co. Ltd. (Shanghai, China). All the reagents used in the present investigation were of analytical grade with no further purification.

2.2. Synthesis of Ce doped ZnO

The precursors of Ce-ZnO were synthesized by hydrothermal method. $Zn(Ac)_2{\cdot}2H_2O$ and $Ce(NO_3)_2.6H_2O$ were used as the zinc source and cerium source. Urea and CTAB were added as precipitant and surface active agent. Ce-ZnO was obtained after calcination. For the typical detailed procedure, $Zn(Ac)_2{\cdot}2H_2O$ (0.2469 g), $Ce(NO_3)_2.6H_2O$ (0.0488 g), urea (0.2704g) and CTAB (0.0474 g) were dissolved into 75 mL distilled water. Then mixed solution was stirred for 30 min and transferred to autoclave with polytetrafluoroethylene liner, followed by reacting for 4 hours at 80°C. Then the solution was further raised to 120°C and heated for another 3 hours. The reaction product was collected, washed with distilled water, dried and calcined at 300°C for 2 hours. Ce doped ZnO samples with different molar ratios of Ce (0.2%, 0.5%, 1%, 5% and 10%) were prepared by changing the content of cerium and repeated the above methods. The samples were denoted as x-Ce-ZnO, where x represents the doping molar ratio of Ce to Zn. For example, the sample was denoted as 0.2%-Ce-ZnO, where molar ratio of Ce to Zn was 0.002.

2.3. Characterization

The morphologies of the Ce-ZnO samples were observed by Hitachi S3400N Scanning electron microscopy (SEM) at an accelerating voltage of 15 Kv, equipped with IXRF energy spectrum analysis (Tec comp. Ltd. China).

X-ray powder diffraction (XRD) patterns were collected in the 2θ range of 5-80° with CuKα radiation (Cu Kα, λ=0.1545 nm, pipe voltage 36 kV, pipe current 20 mA) (Beijing Purkinje General Instrument Co., Ltd., China). Solid-state UV–Vis diffuse reflectance spectra was recorded at room temperature in air by means of a Shimadzu UV-2550 spectrometer equipped with an integrating sphere attachment using $BaSO_4$ as background. UV-Vis spectra of liquid were measured by UV-2600 type ultraviolet visible spectrometer (Shimadzu, Japan).

2.4. Photocatalysis and analysis

The photocatalytic performance of Ce-ZnO two-dimensional nanosheets photocatalysts were assessed by photodegradation of MB solution under visible light irradiation with a 150W halogen lamp. Before the photocatalytic experiment, a mixture of 70 mL MB solution (10 mg/L) and catalyst (10 mg) was vigorously stirred for 30 min to establish an adsorption/desorption equilibrium in the dark. The light source and magnetic stirrer were then opened to do the photocatalytic batch experiments. At given time intervals, 2 mL aliquots were sampled and filtered to remove the solid phase. The filtrates were tested by measuring the absorbance at 665 nm for MB with UV–Vis spectrophotometer.

3. Results and discussion

3.1. XRD patterns

Fig. 1 illustrates the XRD patterns of pure ZnO nanosheets and Ce doped ZnO nanosheets. The XRD pattern of synthesized ZnO was indexed as the pure hexagonal phase of wurtize-type ZnO (JCPDS NO.36-1451) [21, 22]. The diffraction peaks are corresponding to (100), (002), (101), (102), (103) and (200) planes, which is marked in Fig. 1(a). The diffraction peaks of ZnO are broadened gradually and reduced in intensity with increase of Ce doping content, indicating the crystallinity of the ZnO phase is reduced. Doping of Ce causes lattice distortion and defect sites of Zn, weakening the lattice signal of ZnO. No new characteristic diffraction peak is found in the XRD spectrum of Ce-ZnO with 0.2%, 0.5%, and 1% doping. It indicates that no new crystalline was introduced and no phase transition occured. A partial XRD pattern of the Ce doped ZnO nanosheets at a 2θ of 30-34° are shown in Fig. 1(b). It shows clearly that the diffraction peak of the (001) plane of Ce-doped ZnO samples slightly deviates to little angle. It reveals that Ce has substituted some of Zn position in ZnO lattice and causes an expansion of (001) lattice spacing due to larger atomic radius of Ce element [23]. When the content of Ce is larger than 5%, additional peaks appear at $2\theta=28.7^{o}$ in the diffraction patterns of 5%-Ce-ZnO and 10%-Ce-ZnO. The diffraction peak is corresponding to the (111) plane of the cubic CeO_2 crystal. Ce doping saturation of ZnO lattice has been reached with 5% Ce content and new phase of cubic CeO_2 is formed in 5% -Ce-ZnO and 10%-Ce-ZnO nanosheets.

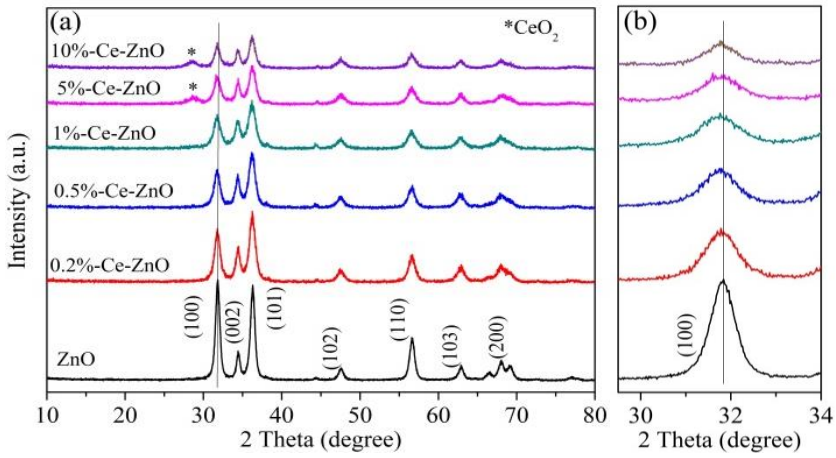

Fig. 1. X-ray diffraction patterns of the samples with different amount of cerium.

3.2. SEM images and EDS analysis

The SEM images of ZnO and Ce-doped ZnO samples are shown in Fig. 2. The morphology of Ce-ZnO samples in Fig. 2(a) exhibits the shape of fish scale-like two-dimensional layered nanosheets. When the sample is locally enlarged, as shown in Fig. 2(b), these nanosheets are about several micrometer in diameter and dozens nanometer thick. The samples keep the similar two-dimensional layered structure when small amount (0.2%, 0.5% and 1%) of Ce were doped, as shown Fig. 2(c), (d) and (e), respectively. Compared with Fig. 2(b), the amplified image of 1%-Ce-ZnO sample in Fig. 2(f) shows that the surface of the naosheets becomes polyporous. Such kind of structure provided abundant active surface area for photocatalytic reaction. The images of 5%-Ce-ZnO (Fig. 2(g)) and 10%-Ce-ZnO (Fig. 2(g)) samples show that the nanosheets collapses into smaller pieces. The layered structures decrease in sizes and become progressively less obvious with the increasing impurity content, which further confirms the decrease of crystallization peak strength in the XRD patterns.

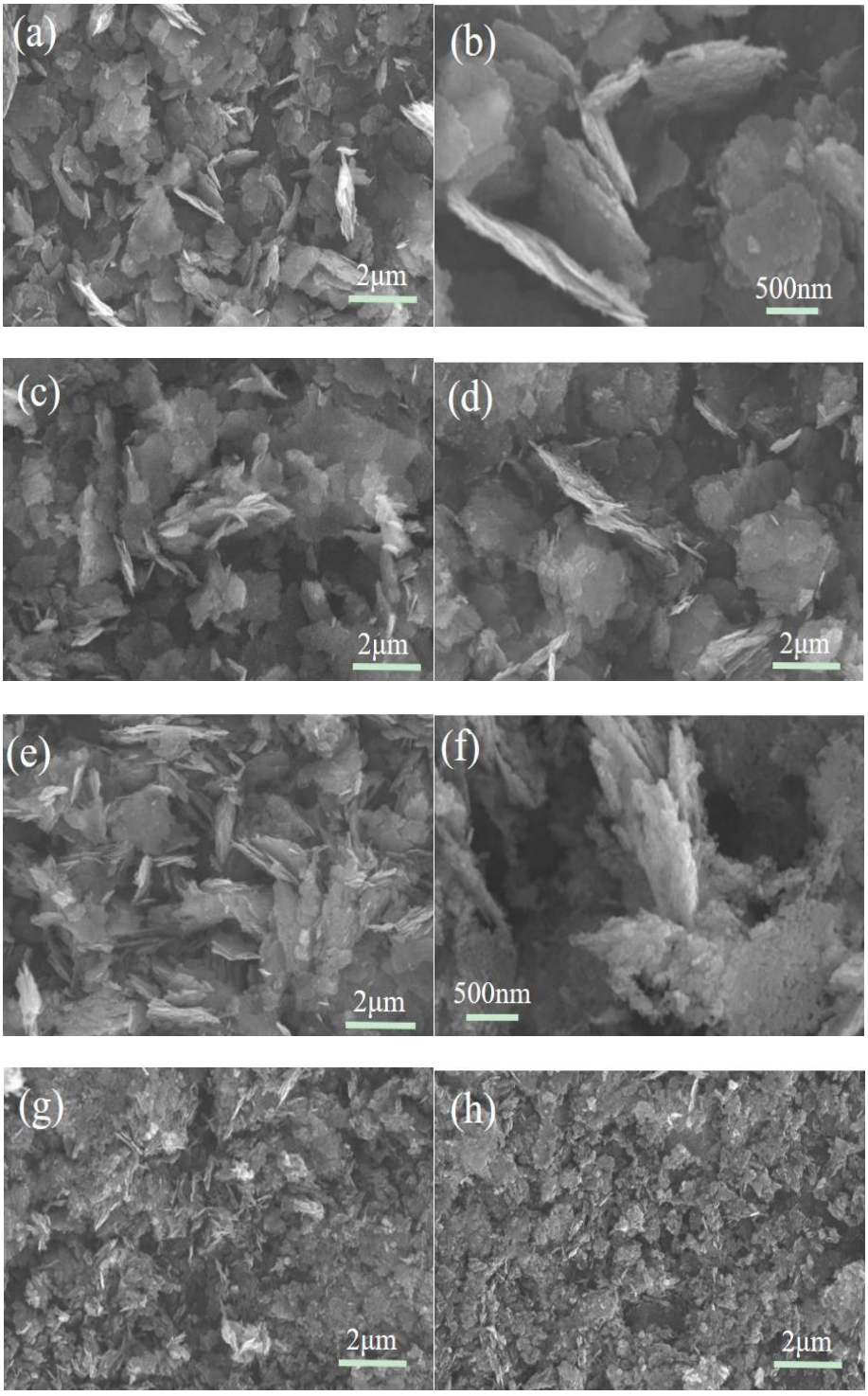

Fig. 2. SEM images of ZnO and Ce doped ZnO (a, b: ZnO , c, d: 0.2 %- Ce-ZnO; e: 0.5%-Ce-ZnO, f:1%-Ce-ZnO, g:5%-Ce-ZnO, h:10%-Ce-ZnO).

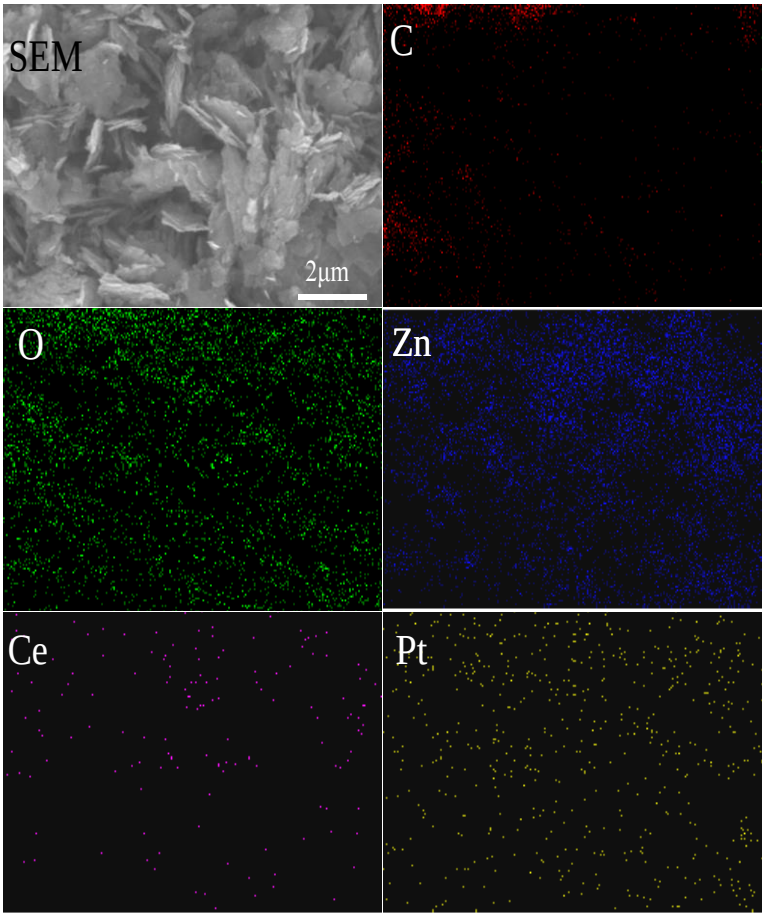

Fig. 3. Elemental mapping of 1 %-Ce-ZnO two-dimensional nanosheets.

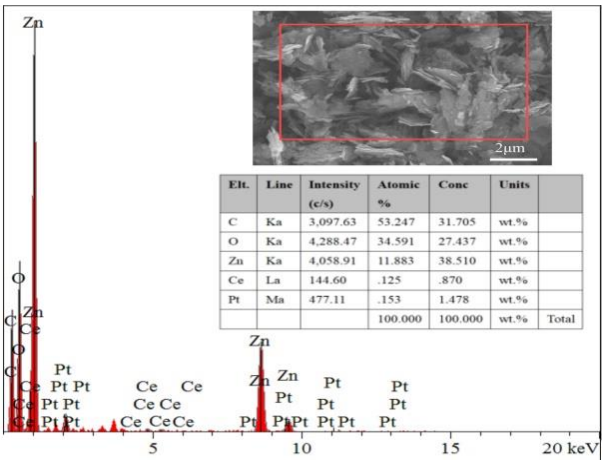

Fig. 4. EDS element spectrum of 1%-Ce-ZnO.

Fig.3 display the SEM image and corresponding C, O, Zn, Ce and Pt elements mapping of 1%-Ce-ZnO sample. The elements Zn, O and Ce distributes evenly all over the sample area. This validated that the Ce have been doped into ZnO successfully. No Ce element segregation have been detected. C and Pt are from the background and Pt sputtering process during SEM sample preparation, respectively. Fig. 4 shows the EDS element spectrum of 1%-Ce-ZnO sample. The EDS element detecting demonstrates the existence of

Zn, Ce and O. The Ce/Zn molar ratio in the table is calculated to be 1.05% (0.125/11.883*100%). This is consistent with the added amount in the experiment.

3.3 UV–Vis DRS analysis

Diffuse Reflectance UV–visible spectra (DRS) of pure ZnO and Ce doped ZnO nanosheets at different Ce contents (0.2%, 0.5%, 1%, 5% and 10% Ce/ZnO molar ratios) are shown in Fig. 5. All the reflectance spectra show a similar shape (Fig. 5a). With the increase of Ce doping amount, The Ce-doped-ZnO exhibitd a slightly enhanced absorption spectrum to longer wavelength within the range of visible light. It is well known that optical absorption properties are associated with its optical energy gap (*Eg*).

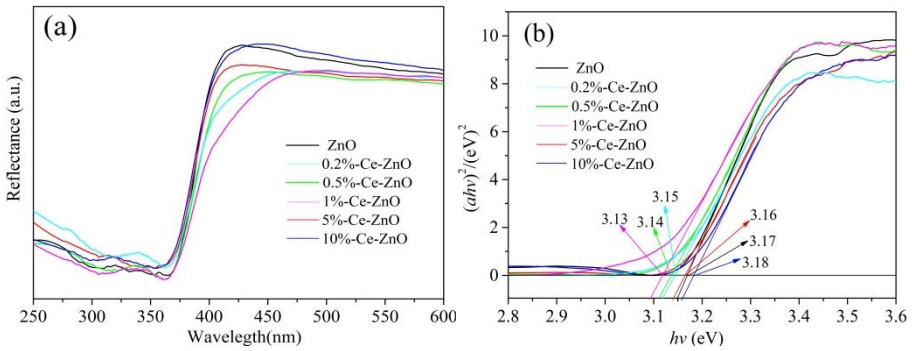

Fig. 5. UV–Vis diffuse reflectance spectra of ZnO and Ce doped ZnO (a), plots of the $(ahv)^2$ versus hv of ZnO and Ce doped ZnO (b).

The band gap energies (*Eg*) were calculated by plotting (*ahv*) *vs* photon energies (*hv*) as shown in Fig. 5(b), where a, h and v represent the absorption coefficient, Planck's constant and light frequency, respectively [24-26]. The Eg of pure ZnO, 0.2%-Ce-Zn, 0.5%-Ce-Zn, 1%-Ce-Zn, 5%-Ce-Zn and 10%-Ce-Zn were determined as 3.15, 3.14, 3.13, 3.16 and 3.18eV, respectively. The Eg value decreased firstly and then increased with increase of the Ce molar ratio in a small range. The broadening of absorption spectrum toward visible light and the decrease of *Eg* samples validated the formation of Ce-ZnO heterostructure [27, 28], which resulted in the enhancement of photocatalytic activity of the Ce doped ZnO nanosheets.

3.4 Photocatalytic Activity of Ce-ZnO

The photocatalytic performance of ZnO and Ce-ZnO nanosheets has been evaluated. The degradation results of methylene blue (MB) (10 mg/L) under visible light radiation are shown in Fig. 6. After 60min of photocatalysis reaction, the residual rate of MB for pure ZnO, 0.2%-Ce-ZnO, 0.5%-Ce-ZnO, 1%-Ce-ZnO, 5%-Ce-ZnO and 10%-Ce-ZnO nanosheets were 20.49%, 15.14%, 8.64%, 3.52%, 25.36% and 27.48%, respectively. In the first 30 minutes of the reaction, the MB content dropped down dramatically and the degradation rate of MB with 1%-Ce-ZnO experiment reached 94.89%. Then the removal rate of MB increased to 96.48% gradually at 60min, which is the highest among six experiment groups. The photocatalytic performance of 0.2%-Ce-ZnO, 0.5%-Ce-ZnO and 1%-Ce-ZnO was better than that of pure ZnO. This is because dopant-induced red shift and increased absorption of visible light spectrum. On the other hand, the polyporous structure of Ce-doped ZnO nanosheet also increased the active surface area significantly. However, the samples of 5%-Ce-ZnO and 10%-Ce-ZnO possessed less photocatalytic activity than pure ZnO. The heterostructures breaks down with excessive content of Ce. Moreover, aggregation of collapsed nanostructures may occur, which result in little surface area of the CeO-ZnO samples. Table.1 shows the photocatalytic efficiency and related paraments of Ce-doped ZnO nanostructures under visible light irradiation from researches [19, 29-31]. Compared with the data from the previous investigation of Ce-doped ZnO nanostructures, the Ce-ZnO

nanosheets synthesized in our work exhibit extraordinarily high photocatalytic performance as well as rapidity of degradation.

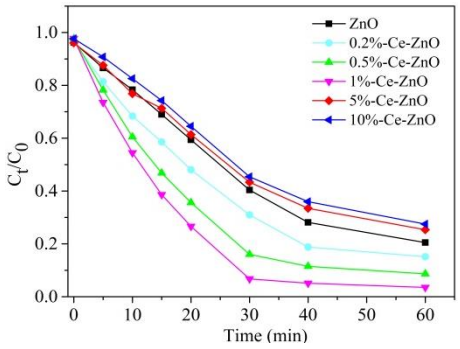

Fig. 6. Photocatalytic activity of MB degradation with pure ZnO and Ce-doped ZnO.

Table 1. the photocatalytic efficiency (MB degradation) of Ce-doped ZnO nanostructures under visible light irradiation.

Photocatalyst	structure	Concentration of dye (ppm)	Amount of Photocatalyst (g/L)	Light irradiation	Degradation efficiency(%)	ph	reference
Ce-ZnO (1%, 3%, 5%, 8%)	Flower-liked nanorods	10	0.4	250w Hg lamp	96.11% in 140 min for 1% Ce-ZnO	-	[29]
Ce-ZnO	Spherical nanoparticles	1	1	Solar light	94.33% in 120min	-	[30]
$Zn_{1-x}Ce_xO$ (x=0,0.02, 0.04,0.06)	Nanobars and nanohexanes	20	0.2	300W visible lamp	94.11% in 60min for X=0.06	12	[19]
Go-Ce-ZnO (7.4%)	Irregular nanoparticles	10	0.6	350 W xenon lamp	99.17% in 90min	-	[31]
Ce-ZnO (0.2%, 0.5%, 1%, 5%, 10%)	Layered nanosheets	10	0.14	150w halogen lamp	96.48% in 60 min for 1% Ce-ZnO	-	Present study

3.5 Effect of pH value

The effect of pH value on 1% Ce-ZnO catalytic oxidation of MB for 60min is shown in Fig.7. When the pH values are 3, 5, 7, 9 and 11, the remaining rates of MB in the solution are 30.69%, 4.79%, 3.52%, 4.16%, and 9.85%, respectively. The photocatalytic effect of 1%-Ce-ZnO on MB is weaker under strong acid conditions (pH=3), which may be due to the acid corrosion induced damage of Ce-ZnO heterostructure. The photocatalytic remaining rates of MB are less than 10% when pH value is in the range of 5 to 11, which further indicates that Ce-ZnO could be used in a wide pH range.

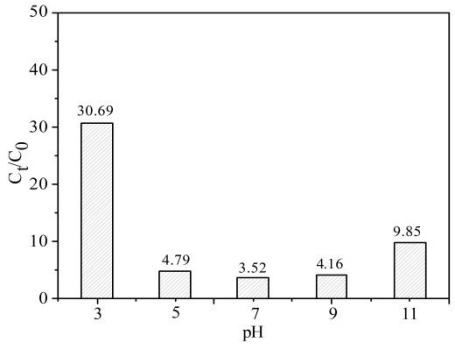

Fig. 7. Effect of pH on Photocatalytic Degradation of MB by 1% Ce-ZnO.

3.6. Catalyst stability

To check the stability of the catalyst, recycle experiments of photocatalytic reaction for 30 min were carried out and the results are presented in Fig. 8. After each run, the catalysts were collected by centrifugation followed ultrasonic cleaning with distilled water. The photocatalytic remaining rates of MB are 6.74%, 9.5%, and 11.8%, respectively. It is observed that the photocatalytic degradation of MB by 1% Ce-ZnO is basically maintained and the catalyst retains its original activity for three recycle experiments, indicating excellent stability.

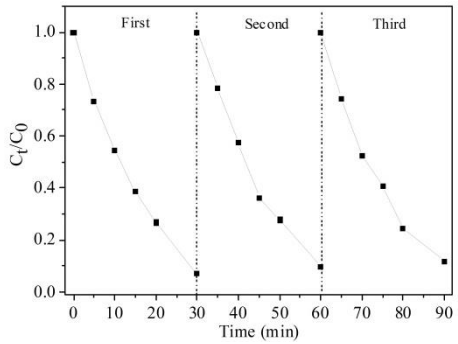

Fig. 8. 1% Ce-ZnO photocatalyst recycles study.

3.7. UV–Vis absorption spectra of MB in photocatalytic reaction

The intermediate products of MB in the photocatalytic degradation experiment group of 1% Ce-ZnO were tested with UV-2600 type ultraviolet visible spectrometer (SHIMADZU Japan) and the results are shown in Fig. 9. As the reaction time prolonged, the maximum absorption peak of MB solution (λ = 664 nm) decreases gradually. Meanwhile, the maximum absorption peak shifts to 654-647 nm. The characteristic peak of 654-647nm is corresponding to azure A. This is because the demethylation reaction of MB took place during at the beginning of photocatalytic degradation of MB. A methyl is removed from MB molecules to form azure A, so that the blue shift occurs. The results of photocatalytic degradation of MB are in agreement with those reported in the literature [32, 33]. The degradation curve of 60min indicated that MB has been totally oxidized eventually with no absorption peak.

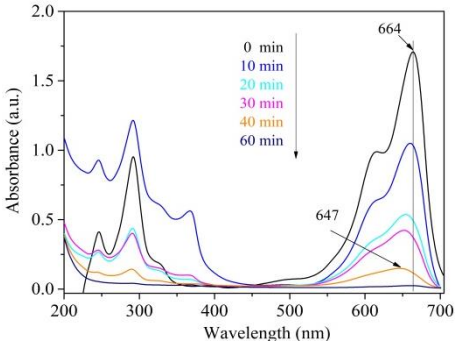

Fig. 9. UV–Vis absorption spectra of MB in photocatalytic reaction.

3.8. Photocatalytic mechanism

The degradation of MB is considered to be that the hydroxyl radical produced acts on MB. It is also considered that the degradation of MB is associated with hole electrons (e^-/h^+) [34]. In order to study the active oxide species in the photocatalytic oxidation degradation of MB, the holes trapping agent ethylene diamine tetraacetic acid disodium salt (EDTA-2Na) and a hydroxyl radical trapping agent isopropanol (IPA) were added to the 1%-Ce-ZnO reaction system [33, 35]. Therefore, in the reaction system, the photocatalytic degradation experiment was carried out according to the initial concentration of MB and the molar ratio of IPA (or EDTA-2Na) to MB was 200:1. The results are shown in Fig. 10. The residual rate of MB is 3.52% in the 1%-Ce-ZnO photocatalytic oxidation system after 60 min. while the residual rate of MB is 76.07% and 83.6%, respectively, when IPA and EDTA-2Na are added to the system mentioned above. This indicates that when adding IPA and EDTA-2Na, the degradation of MB is hindered. As a result, h^+ and ·OH are the active oxidation species in the photocatalytic process of MB.

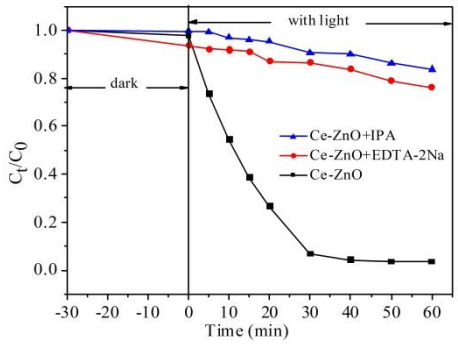

Fig. 10. Effect of different capture agents on catalytic degradation of MB.

Based on the theory of solid band and the mechanism of semiconductor photocatalysis, we speculate the possible mechanism of photocatalytic degradation of MB. Photogenerated electrons (e^-) and holes (h^+) are generated on the surface of the photocatalyst Ce-ZnO during irradiation (Eq. (1)). The photo induced h^+ oxidizes the H_2O molecule, which is in the reaction system, into ·OH species (Eq. (2)). The photo induced e^- interacts with the O_2 molecule, adsorbed on the surface of the catalyst, to form superoxide anion $\cdot O_2^-$ (Eq.(3)). In addition, $\cdot O_2^-$ and H^+ react to form the proxygene ion HO_2^- (Eq.(4)), and the generated HO_2^- and H^+ react to form H_2O_2 (Eq.(5)), H_2O_2 produces ·OH under light conditions (Eq. (6)). The ·OH generated in the system acts on the oxidation of MB molecules into small molecules (Eq. (7)).

$$\text{Ce-ZnO} + h\nu \rightarrow \text{ZnO}(e^- + h^+) \quad (1)$$

$$h^+ + H_2O \rightarrow \cdot OH + H^+ \quad (2)$$

$$e^- + O_2 \rightarrow \cdot O_2^- \quad (3)$$

$$\cdot O_2^- + H^+ \rightarrow HO_2^- \quad (4)$$

$$HO_2^- + H^+ \rightarrow H_2O_2 \quad (5)$$

$$H_2O_2 + h\nu \rightarrow 2\cdot OH \quad (6)$$

$$\cdot OH + MB \rightarrow \text{Degradation products} \quad (7)$$

When IPA is added to the reaction system, the ·OH is captured. Since the degradation process of MB is inhibited, the residual rate of MB in the solution increases remarkably. When the EDTA-2Na is added, the Reaction (2) is hindered, which would hinder the degradation of MB as well. Although the h^+ is captured, the Reaction (1) can be made to the right side, which leads to the production of a large amount of e^- at the surface and inside of the catalyst. The photo induced e^- and O_2 in the solution to produced $\cdot O_2^-$ according to Reaction (3). The $\cdot O_2^-$ and H^+ in the solution are to produce the intermediate substance HO_2^-, according to Reaction (4). The above HO_2^- subsequently to produce ·OH according to the Reactions (5) and (6), so the ·OH generated by the e^- action can continue to act on the MB. Thus, the extent of obstruction of photocatalytic experiment of MB with EDTA-2Na is not obvious as that with IPA. This is consistent with the experimental results.

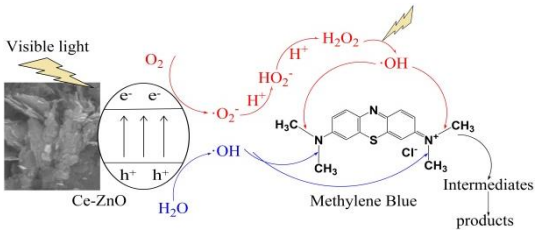

Fig. 11. The possible mechanism for photocatalytic degradation of MB with Ce-ZnO.

According to the above discussion, combined with the analysis of UV-Vis absorption spectra, the possible mechanism for photocatalytic degradation of MB with Ce-ZnO is proposed (as shown in Fig. 11). Under visible light irradiation, the Ce-ZnO heterostructure is excited and electrons in valence band transfer to the conduction band to produce e^- and h^+. These e^- and h^+ can move freely in the catalyst. Since the polyporous nanosheets structure provides sufficient active surface area, the e^- and h^+ can easily migrate in the surface. Then e^- reacts with O_2 in the solution to produce $\cdot O_2^-$. The above $\cdot O_2^-$ and H^+ in the solution finally produce ·OH. On the other hand, h^+ in the valence band reacts with H_2O to generate ·OH. These active species mentioned above then act on MB, cause it to undergo demethylation, and oxidize it to small molecules, so as to achieve the purpose of decolorization and degradation of MB.

4. Conclusion

The Ce-doped ZnO two-dimensional nanosheets were successfully prepared by hydrothermal method. The XRD patterns demonstrated that the ZnO nanosheets kept highly crystallinity and Ce ions were successfully incorporated into the lattice position of ZnO. The morphology of ZnO layered nanosheets with low Ce doped content (<1%) showed a

fish-scale liked polyporous structure, whereas the sheets collapsed to smaller pieces when the Ce doping mole ratio increase to 5%. 1%-Ce-ZnO nanosheets exhibited the highest degradation efficiency for removal of MB due to the formation of Ce-ZnO heterostructure and the increase of active surface area. The MB degradation rated reached 96.48% after 60min visible light irradiation.1%-Ce-ZnO nanosheets kept high photocatalytic performance at a wide pH range of 5-11. The mechanism investigation photocatalytic degradation of MB showed the photocatalytic degradation reaction initiated from the demethylation of MB and the h^+ and $\cdot OH$ acted as key active species during the oxidation of MB. The Ce doped ZnO nanosheets in this work showed high photocatalytic performance of degradation of organic pollutants, high rapidity and superior recyclability. These make the Ce-ZnO nanosheets to be a powerful tool to deal with the wastewater containing organic contaminants.

Acknowledgements

This work is supported by Zhejiang Provincial Natural Science Foundation of China (LQ19E040001 and LQ20E040001). The work is also supported by Research fund of Huzhou University (2019XJKJ33).

References

[1] Shi, L., K. Zhao, S. Liu, Materials Letters **228**, 121 (2018).
[2] M. Wang et al., Journal of Hazardous Materials **347**(APR.5), 403 (2018).
[3] A. B. Ahmed et al., Applied Catalysis B Environmental **156-157**, 456 (2014).
[4] D. Zhu, Q. Zhou, Environmental Nanotechnology, Monitoring & Management **12**, 100255 (2014).
[5] M. R. Al-Mamun et al., Journal of Environmental Chemical Engineering **7**(5), 103248 (2019).
[6] Y. U. Hang et al., Bulletin of Materials Science **36**(3), 367 (2013).
[7] Chunlian et al., Journal of Alloys & Compounds An Interdisciplinary Journal of Materials Science & Solid State Chemistry & Physics, 2014.
[8] Q. Ma et al., Journal of materials **30**(3), 2309 (2019).
[9] A. Srivastava, N. Kumar, S. Khare, Nephron Clinical Practice **22**(1), 68 (2013).
[10] H. Abdelkader et al., Effect of La Doping on ZnO Thin Films by Spray Pyrolysis, Defect and Diffusion Forum, 2019.
[11] M. Caglar et al., Journal of Materials Science Materials in Electronics **19**(8-9), 704 (2008).
[12] G. Krishna Reddy et al., Journal of Asian Ceramic Societies, S2187076417300787 (2017).
[13] D. W. Zeng et al., Journal of Crystal Growth **266**(4), 511 (2004).
[14] Q. Wan et al., Optical Materials **30**(6), 817 (2008).
[15] F. Achouri et al., Materials & Design **101**, 309 (2016).
[16] Z. Shen et al., J Colloid Interface Sci. **556**, 726 (2019).
[17] K. T. Ranjit et al., Environmental Science & Technology **35**(7), 1544 (2001).
[18] C. J. Chang, C. Y. Lin, M. H. Hsu, Journal of the Taiwan Institute of Chemical Engineers **45**(4), 1954 (2014).
[19] Sukriti et al., Vacuum, 109364 (2020).

[20] J. Jiang et al., Journal of Alloys & Compounds **699**, 907 (2017).
[21] L. Fang et al., Superlattices & Microstructures **75**, 324 (2014).
[22] N. P. Subiramaniyam et al., Journal of Materials Science Materials in Electronics **28**(21), 1 (2017).
[23] J. Ryu, H. Lee, Applied Physics Letters **105**(11), 111903(2014).
[24] Sundaram Chandrasekaran et al., Chemical Society Reviews **48**, (2019).
[25] D. P. Singh et al., The Journal of Physical Chemistry C **111**(4), 1638 (2007).
[26] M. A. Butler, D. S. Ginley, Journal of The Electrochemical Society **125**(2), 228 (1978).
[27] C. Qin et al., Journal of Alloys and Compounds **770**, 972 (2019).
[28] M. Khatamian et al., Journal of Molecular Catalysis A: Chemical **365**, 120 (2012).
[29] L. Wang et al., Materials Science in Semiconductor Processing **71**, 401 (2017).
[30] N. Kannadasan et al., Materials Characterization **97**, 37 (2014).
[31] Y. N. Wang, J. Li, Q. Wang, Optik **204**, 164131 (2020).
[32] T. Zhang et al., Journal of Photochemistry & Photobiology A Chemistry **140**(2), 163 (2001).
[33] M. Xu et al., Applied clay **170**(MAR.), 46 (2019).
[34] Meng et al., Applied Catalysis B Environmental An International Journal Devoted to Catalytic Science & Its Applications, 2016.
[35] Yan et al., Journal of Alloys & Compounds An Interdisciplinary Journal of Materials Science & Solid State Chemistry & Physics, 2016.